Chinese Chemical Letters 34 (2023) 107544

Contents lists available at ScienceDirect

Chinese Chemical Letters

journal homepage: www.elsevier.com/locate/cclet

Revealing milling durations and sintering temperatures on conductivity and battery performances of $Li_{2.25}Zr_{0.75}Fe_{0.25}Cl_6$ electrolyte

Shuai Chen[a,b], Chuang Yu[a,*], Chaochao Wei[a], Linfeng Peng[a], Shijie Cheng[a], Jia Xie[a,*]

[a] State Key Laboratory of Advanced Electromagnetic Engineering and Technology, School of Electrical and Electronic Engineering, Huazhong University of Science and Technology, Wuhan 430074, China
[b] School of Materials, Huazhong University of Science and Technology, Wuhan 430074, China

ARTICLE INFO

Article history:
Received 5 April 2022
Revised 28 April 2022
Accepted 18 May 2022
Available online 22 May 2022

Keywords:
Solid inorganic electrolyte
Solid state battery
Halide electrolyte
High temperature
Synthesis process

ABSTRACT

Halide electrolytes in solid-state batteries with excellent oxidative stability and high ionic conductivity have been well reported recently. However, the high-cost rare-earth elements and long duration of high-rotation milling procure are the major obstacles. Herein, we have successfully synthesized the low cost $Li_{2.25}Zr_{0.75}Fe_{0.25}Cl_6$ electrolyte consisting of abundant elements with comparable Li-ion conductivity in a short milling duration of 4 h. Phase transition of the annealed sample was also carefully investigated. $LiNi_{0.6}Co_{0.2}Mn_{0.2}O_2/Li_{2.25}Zr_{0.75}Fe_{0.25}Cl_6/Li_{5.5}PS_{4.5}Cl_{1.5}$/In-Li batteries using different halide electrolytes were constructed and cycled at different voltage windows. Solid-state battery using $Li_{2.25}Zr_{0.75}Fe_{0.25}Cl_6$ electrolyte obtained from long milling duration delivers higher discharge capacities and superior capacity retention than shorter milling time between 3.0 and 4.3 V. It delivers much higher discharge capacity when cycled at elevated temperature (60 °C) and suffers fast capacity degradation when the upper cut-off voltage increases to 4.5 V at the same current density. This work provides an efficiency synthesis strategy for halide solid electrolyte and studies its applications in all-solid-state batteries in a wide temperature range.

© 2023 Published by Elsevier B.V. on behalf of Chinese Chemical Society and Institute of Materia Medica, Chinese Academy of Medical Sciences.

All-solid-state lithium batteries (ASSLBs) with high safety and energy densities show great potential as next generation energy storage system in electric transport and smart grid [1]. However, the low ionic conductivity and poor stability of current solid electrolytes limit their applications in solid-state batteries. Intensive efforts have been imputed to exploring new kinds of solid electrolytes [2]. Oxide electrolytes show high chemical stability towards both cathode and lithium metal anode, while those materials suffer low ionic conductivity, poor mechanical handling property and large solid-solid interface resistances [3,4]. Polymers and hydride electrolytes have good mechanical flexibility and lithium compatibility, but their limited ionic conductivity leading to poor battery performances [5,6]. Sulfide electrolytes are the first families that showing ultrahigh ionic conductivity even higher than that of organic liquid electrolytes [7–9]. The good mechanical property and small interfacial resistance towards electrode materials makes sulfide electrolytes a suitable electrolyte for ASSLBs. However, the moisture sensitivity, narrow charge/discharge voltage window and low chemical/electrochemical stability with commercial cathode materials are critical obstacles for its applications [10–14].

Halide electrolytes with excellent pristine cathode stability, acceptable ionic conductivity, and good mechanical strength have significantly attracted attentions. Tetsuya Asano *et al.* [15] have successfully synthesized Li_3YCl_6 and Li_3YBr_6 electrolytes with high conductivities of 0.51 and 0.72 mS/cm using the mechanical milling routes. Afterwards, many kinds of Li_3MX_6-type halide electrolytes have been designed and prepared, such as Li_3InCl_6 [16], Li_3ErCl_6 [17]. Sun *et al.* found that Li_xScCl_{3+x} electrolytes show the highest ionic conductivity of 3 mS/cm when $x=3$ [18]. Recently, Zhou *et al.* reported spinel structure $Li_2In_xSc_{0.666-x}Cl_4$ electrolytes with excellent cycling performance between a high voltage window up to 4.8 V when combined with NCM85 cathode and In-Li anode [19]. However, large amount of high-cost rare-earth in the composition of those reported halide electrolytes impede their widely application in ASSLBs. Wang *et al.* reported a new kind of halide electrolyte Li_2ZrCl_6 with comparable conductivity and consisting of high abundant zirconium, which greatly decrease the cost [20]. Multiple substation strategies have been applied to explore new kinds of low-cost halide electrolytes, such as

* Corresponding authors.
E-mail addresses: cyu2020@hust.edu.cn (C. Yu), xiejia@hust.edu.cn (J. Xie).

https://doi.org/10.1016/j.cclet.2022.05.058
1001-8417/© 2023 Published by Elsevier B.V. on behalf of Chinese Chemical Society and Institute of Materia Medica, Chinese Academy of Medical Sciences.

$Li_{2.25}Zr_{0.75}Fe_{0.25}Cl_6$ [21], $Li_{2+x}Y_xZr_{1-x}Cl_6$ [22], $Li_{2+x}Yb_xZr_{1-x}Cl_6$ [23]. Our previous work has successfully increased the ionic conductivity of Li_2ZrCl_6 up to 10^{-3} S/cm *via* the replacement of Zr^{4+} with In^{3+} in the structure [24].

Although the water-meditated synthesis route has been reported by Li *et al.* [25,26], most of those reported halide electrolytes are synthesized using the solid-state synthesis method. To obtain the target phase, high rotation milling process was typical chosen to prepare those halide electrolytes. The common synthesis procure is to mill the mixture of starting materials with high-rotation speed for long durations. Schlem *et al.* have tailored the synthesis processes of Li_3ErCl_6 and Li_3YCl_6 when using the solid-state reaction method to achieve high ionic conductivity [17]. This long milling period is time and energy consuming and lowers the repeatability of the obtained halide electrolytes, limiting their large-scale synthesis and applications. The mechanical milling process plays a key role on the variability of the cationic in the structure. Moreover, the phase impurity and amorphous content are decided by the milling durations, which also affect the corresponding electrochemical performances. Unraveling the influence of milling durations in Li-ion conductivity and battery performances of halide electrolytes can accelerate their application.

For some inorganic solid electrolytes synthesized using the mechanical milling process, a higher crystallinity normally provides a faster ion diffusion [27], which has also been confirmed by our previous work [28]. Heat treatment is the typical post handling method to enhance the crystallinity of solid electrolyte prepared by high rotation milling process. However, some halides electrolytes $Li_xM_yCl_6$ have reported have much lower ionic conductivity after heat treatment (*e.g.*, $Li_{3-x}Yb_{1-x}M_xCl_6$ [23], Li_2ZrCl_6 [20]). When some others can obtained high ionic conductivity samples through heat treatment (*e.g.*, $Li_3InCl_{4.8}F_{1.2}$ [29], Li_3YBr_6 [30]). While the sintering process on the phase transition and ionic conductivity of $Li_{2.25}Zr_{0.75}Fe_{0.25}Cl_6$ is unclear.

Halide Li_3MX_6 electrolytes have been reported to show a high electrochemical stability towards active cathode materials and a wide charging/discharging voltage window [31]. However, the actual cathode and electrolyte stability of halide electrolytes at higher cut-off voltage under elevated operating temperatures still needs to be confirmed [32]. High operating temperatures provide faster ionic conductivity for solid electrolyte and also suffer more intense side reactions and interfacial stability, which may become more serious under higher upper cut-off voltages.

Herein, we successfully synthesize large amounts of $Li_{2.25}Zr_{0.75}Fe_{0.25}Cl_6$ (LZFC) electrolyte with high Li-ion conductivity of 0.80 mS/cm at room temperature through the simple ball-milling strategy. Although the short-term milling also can provide comparable Li-ion conductivity (0.74 mS/cm), the corresponding electrochemical performances in solid-state batteries are totally different. The influence of sintering treatment in the phase transition of the obtained LZFC electrolyte has also been studied. Solid-state batteries using those two kinds of LZFC electrolytes and $Li_{5.5}PS_{4.5}Cl_{1.5}$ buffer layer, combined with the $LiNi_{0.6}Co_{0.2}Mn_{0.2}O_2$ cathode and Li-In anode have been constructed. Electrochemical performances at different voltage windows and different operating temperatures are carefully investigated. Multiple characterization methods, including XRD, *dQ/dV*, and EIS are performed to unravel the working mechanism of those assembled batteries cycled at different operating conditions.

To prepare the $Li_{2.25}Zr_{0.75}Fe_{0.25}Cl_6$ electrolyte, the mixture of starting materials was ball-milled using the WC balls and jars. The total weight of the raw materials was fixed at 20 g. Fig. 1a shows XRD patterns of the LiCl, $FeCl_3$ and $ZrCl_4$ mixture from the beginning to 16 h. As depicted in Fig. 1a, the diffraction peaks of the raw mixture after 110 rpm are indexed to the standard XRD peaks of those starting materials. After 4 h milling, those XRD peaks are indexed well to the pure Li_3YCl_6 structure. With increasing milling durations, no clear impurity phase is observed in the XRD patterns, suggesting that the pure target phase of LZFC electrolyte has been successfully synthesized after 4 h. The sample milled after 16 h shows similar reflections in the XRD patterns as that obtained after 4 h, both of which can be indexed to the Li_3YCl_6 structure with a space group of $p\bar{3}m1$. The corresponding crystal structure of LZFC is depicted in Fig. 1b. To investigate the ionic conductivity changes during the milling process, the mixture after different milling durations was measured using the AC impedance using stainless steel as the blocking electrode. As presented in Fig. 1c, the mixture shows a decrease of resistance in the first 4 h, from 174.1 Ω for the mixture after 110 rpm to 88.3 Ω for the mixture after 550 rpm for 4 h. In the subsequent milling processes, the mixture displays slightly changed resistance, resulting in a resistance of 93.1 Ω for 8 h, 71.9 Ω for 12 h, and 82.3 Ω for 16 h, respectively. The corresponding Li-ion conductivities of those mixtures deduced from the resistances in Fig. 1d are 0.75, 0.71, 0.86 and 0.80 mS/cm for 4, 8, 12 and 16 h milling. The comparable conductivity of the mixture milled after 4 h and 16 h, suggests that this kind of halide solid electrolytes can be easily prepared after a short milling duration. Although our result is slightly lower than the previous result, a much larger amount (20 g) of the target material in one batch with comparable ionic conductivity (0.98 mS/cm *vs.* 0.74 mS/cm) was successfully synthesized in a shorter high rotation milling duration (4 h *vs.* 10 h) [21]. XPS spectra of LZFC in Fig. 1e show the same Zr 3d and Cl 2p peaks as previously reported in Fig. 1e, confirming similar surface conditions of our sample compared to the previous sample [14,15].

Previous research has reported that the site disorder decreases during the annealing process for some halide solid electrolytes, resulting in increased activation barriers for ion diffusion and lowered Li-ion conductivities. To unravel the influence of post heat treatment in the phase transition and ionic conductivity variations of our halide electrolytes, the obtained LZFC from the mechanical milling process was sintered at different temperatures for 5 h. As shown in Fig. 2a, the diffraction peaks located at 16.2° and 32.5° become weaker and a new XRD peak located at 15.1° appears for the sample annealed at 350 °C, indicating a phase transition of the milled sample from the hcp Li_3YCl_6 phase to the ccp Li_3InCl_6 phase [9,10]. When the annealing temperature reaches 450 °C and even higher temperatures, the XRD diffractions are indexed to the ccp Li_3InCl_6 phase. After the sintering process, the obtained sample in the quartz tube shows a clear melting recrystallization phase. The higher annealing temperature provides high crystallinity for the corresponding sintered LZFC electrolyte. The ionic conductivities of the annealed samples were measured at different recording temperatures using the AC impedance. As depicted in Fig. 2b, the annealed samples show much higher resistances at room temperature than that of the milled LZFC electrolyte. As shown in Fig. 2c, after the sintering process, the ionic conductivity of the milled LZFC sample suffers a rapidly decrease, from 0.74 mS/cm to 3.1×10^{-5} S/cm at 350 °C, 2×10^{-6} S/cm at 450 °C, 1.2×10^{-5} S/cm at 550 °C, and 9.0×10^{-6} S/cm at 650 °C, respectively. Interestingly, those annealed samples show new arcs in the spectra at room temperature and become more obvious when the recording temperature increases, suggesting a multiphase is formed during the annealing process. Fig. 2d displays the Arrhenius plot of the milling and sintering samples. The activation energies were deduced from the temperature-dependent conductivities. The obtained activation energy for the milled sample is 0.28 eV. After the annealing process, the sintered samples show activation energies of 0.44 eV, 1.07 eV, 0.59 eV and 0.58 eV when annealed at 350 °C, 450 °C, 550 °C and 650 °C, respectively. The highest activation energy is achieved when the sintering temperature is 450 °C, sug-

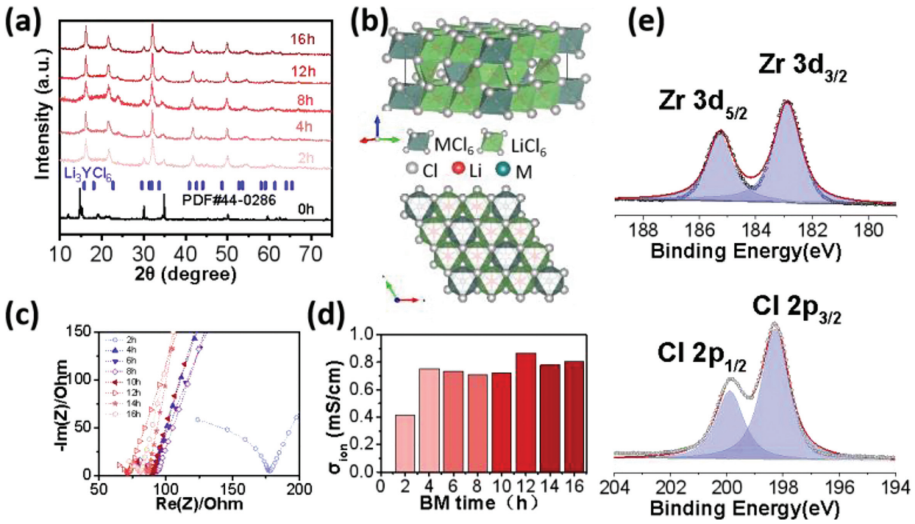

Fig. 1. (a) XRD patterns of $Li_{2.25}Zr_{0.75}Fe_{0.25}Cl_6$ obtained after different milling durations. (b) Crystal structure schematic diagram of $Li_{2.25}Zr_{0.75}Fe_{0.25}Cl_6$ electrolyte. (c) Nyquist impedance spectra of the sample milled for different periods measured at room temperature and (d) the corresponding Li-ion conductivity of different $Li_{2.25}Zr_{0.75}Fe_{0.25}Cl_6$ electrolytes. (e) XPS patterns of $Li_{2.25}Zr_{0.75}Fe_{0.25}Cl_6$ electrolyte obtained after milling for 4 h.

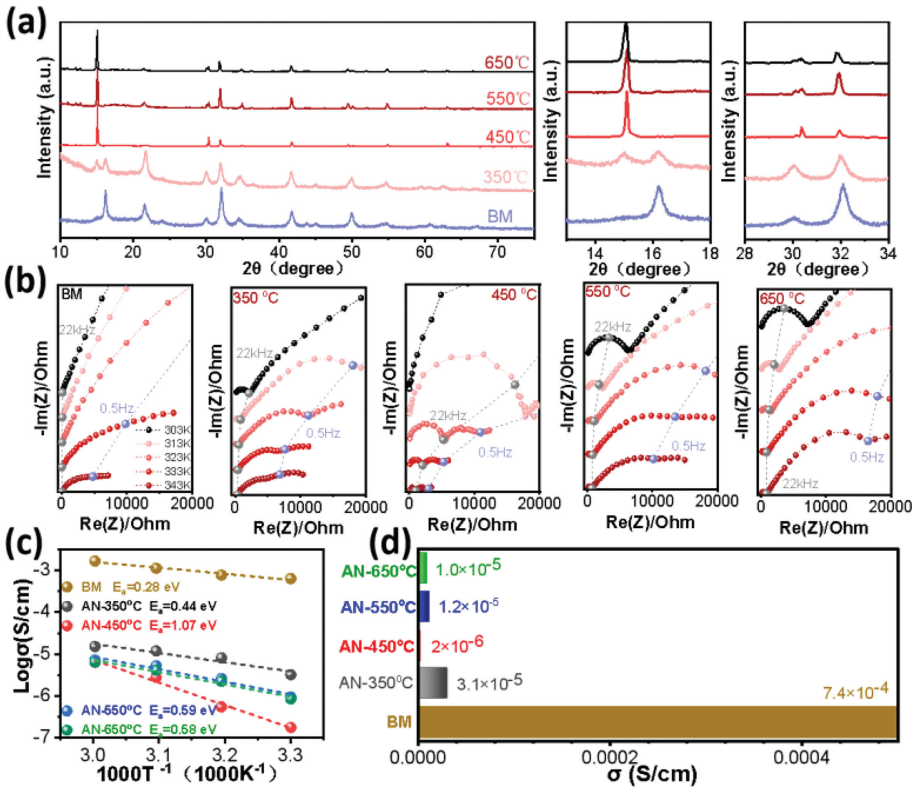

Fig. 2. (a) XRD patterns of the milled $Li_{2.25}Zr_{0.75}Fe_{0.25}Cl_6$ electrolytes annealing at different temperatures for 5 h. (b) Nyquist impedance spectra of different samples obtained after annealing process measured at different recording temperatures. (c) The ionic conductivity and (d) Arrhenius plot of these electrolytes.

gesting that the recrystallization temperature is nearby this temperature.

To compare the electrochemical performances of the obtained LZFC solid electrolytes milled after 4 h and 16 h, the bare $LiNi_{0.6}Co_{0.2}Mn_{0.2}O_2$ cathode and Li-In anode was chosen to combine with the above solid electrolytes to fabricate all-solid-state batteries and the corresponding battery performances were investigated. However, the halide solid electrolytes have been reported to show poor stability towards both the bare Li metal and Li-In anode [33]. Our LZFC electrolyte also suffers this issue. Therefore, chlorine-rich argyrodite $Li_{5.5}PS_{4.5}Cl_{1.5}$ electrolyte with both ultrahigh Li-ion conductivity (comparable to the conductivity of current liquid electrolyte) and good compatibility with Li-In anode was chosen as the buffer layer to separate the direct contact between the halide electrolyte and anode materials. The $LiNi_{0.6}Co_{0.2}Mn_{0.2}O_2/Li_{2.25}Zr_{0.75}Fe_{0.25}Cl_6/Li_{5.5}PS_{4.5}Cl_{1.5}$/In-Li solid-state batteries with different kinds of LZFC electrolytes were constructed and cycled at a current density of 0.161 mA/cm^2 (0.2 C) in the voltage range of 3.0–4.3 V *vs.* Li^+/Li^0. As shown in Fig. 3a, all-solid-state batteries using $Li_{2.25}Zr_{0.75}Fe_{0.25}Cl_6$ electrolytes milled after 4 and 16 h deliver initial discharge capacities of 133.7 and 153.1 mAh/g with corresponding coulombic efficiencies of

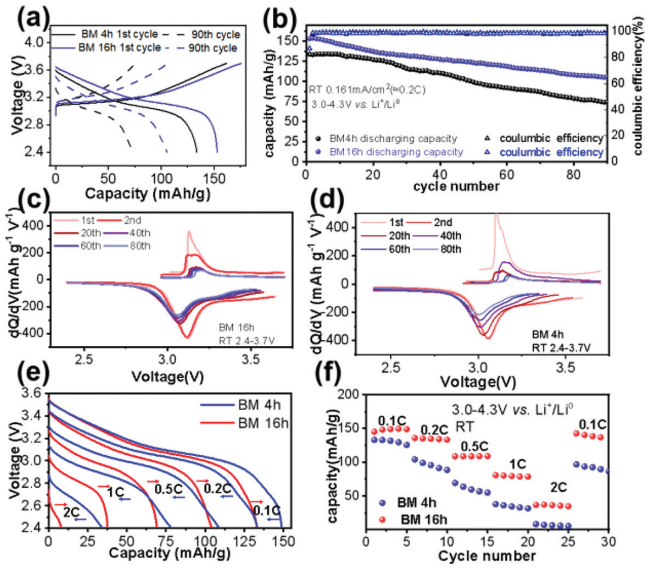

Fig. 3. (a) The initial and 90th charge/discharge curves and (b) the corresponding cycling performances of NCM622/$Li_{2.25}Zr_{0.75}Fe_{0.25}Cl_6$/$Li_{5.5}PS_{4.5}Cl_{1.5}$/In-Li solid-state batteries cycled at 0.2 C under room temperature between 3.0 V and 4.3 V (*vs.* Li^+/Li^0). (c) The d*Q*/d*V* curves of the chosen cycles for the battery with electrolyte BM 16 h and (d) BM 4 h under room temperature. (e) Discharging curves and (f) rate capability of the above solid-state batteries cycled at different C-rates, 0.1 C, 0.2 C, 0.5 C, 1 C and 2 C, respectively. For those solid-state batteries cycled in this figure, the $Li_{2.25}Zr_{0.75}Fe_{0.25}Cl_6$ electrolyte obtained after 4 h and 16 h were chosen as solid electrolytes, respectively.

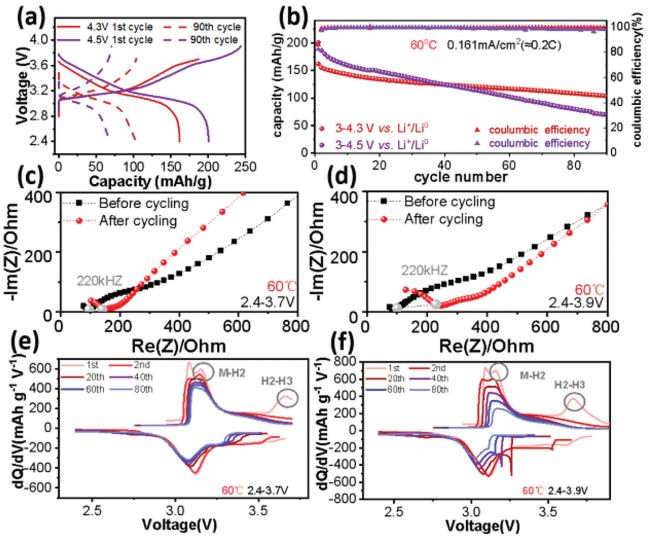

Fig. 4. (a) The 1st charge/discharge curves and (b) the cycling performances of NCM622/$Li_{2.25}Zr_{0.75}Fe_{0.25}Cl_6$/$Li_{5.5}PS_{4.5}Cl_{1.5}$/In-Li solid-state batteries cycled between different cut-off voltage windows at 0.2 C under 60 °C. (c) EIS spectrum of the assembled battery before and after 90 cycles cycling at 3.0–4.3 V and (d) 3.0–4.5 V *vs.* Li^+/Li^0. (e) The d*Q*/d*V* curves of the chosen cycles for the battery cycling at 3.0–4.3 V and (f) 3.0–4.5 V *vs.* Li^+/Li^0 under 60 °C.

82.62% and 86.99%, respectively. After 90 cycles, those batteries maintain discharge capacities of 74.9 and 105.5 mAh/g with capacity retentions of 56.0% and 68.6%, respectively, as shown in Fig. 3b. During cycling tests, both batteries show high coulombic efficiencies up to 99% in the figure, suggesting excellent lithium intercalation/ deintercalation behaviors. To investigate the phase transition of the cathode during cycling with different electrolytes, the d*Q*/d*V* plots of the above batteries cycled at the fixed cycles are compared as shown in Figs. 3c and d. Similar d*Q*/d*V* peaks locate at ~3.08 and 3.06 V are observed during the initial charging/ discharging processes. However, the *dQ/dV* peaks of the assembled battery using electrolyte obtained by milling after 16 h overlap better than that of short period milling electrolyte during the subsequent cycles, suggesting superior cyclability. To investigate the structural variations of active material in cathode mixture before and after cycles, the cycled cathodes were collected and characterized with powder XRD. As depicted in Fig. S1a (Supporting information), the diffraction peaks of cathode mixtures of both batteries cycled between 3.0 V and 4.3 V (*vs.* Li^+/Li^0) are indexed well with the R3m layered structure and no impurity phases are observed from the pattern, suggesting the good structural maintainability when cycled with $Li_{2.25}Zr_{0.75}Fe_{0.25}Cl_6$ electrolytes. This agrees well with previous result that halide electrolyte possess excellent cyclability with pristine high-voltage cathode [32].

Additionally, the rate capability of those assembled solid-state batteries using different $Li_{2.25}Zr_{0.75}Fe_{0.25}Cl_6$ electrolytes measured at room temperature was also carefully investigated. As depicted in Fig. 3e, when the charge/discharge rate increases step-by-step from low C-rate (0.1 C) to high C-rate (2 C), the discharge capacity decreases obviously. The solid-state battery using $Li_{2.25}Zr_{0.75}Fe_{0.25}Cl_6$ electrolyte milled after 4 h delivers discharge capacities of 133.1 mAh/g at 0.1 C, 104.1 mAh/g at 0.2 C, 69.1 mAh/g at 0.5 C, 37.7 mAh/g at 1 C, and 8 mAh/g at 2 C. In contrast, solid-state battery using $Li_{2.25}Zr_{0.75}Fe_{0.25}Cl_6$ electrolyte milled after 16 h shows much higher discharge capacities at the rates, 148.1 mAh/g at 0.1 C, 135.8 mAh/g at 0.2 C, 108.7 mAh/g at 0.5 C, 80.1 mAh/g at 1 C, and 142.7 mAh/g at 2 C, respectively. With increasing charge/discharge rates, the discharge curves of both batteries exhibit clear degradation of discharge voltage plateaus in Fig. 3e. As shown in Fig. 3f, the battery using solid electrolyte with a longer milling duration (16 h) is attributed to the smaller particle sizes, which agrees well with our previous work [34].

Furthermore, the assembled ASSLBs were cycled in a wider voltage window of 3.0–4.5 V (*vs.* Li^+/Li^0) to evaluate the electrochemical performances. As shown in Fig. S3a (Supporting information), a slight voltage platform appears at 4.25 V (*vs.* Li^+/Li^0). Moreover, this battery delivers an initial discharge capacity of 141.1 mAh/g and suffers a rapid degradation in the subsequent cycles. After 80 cycles, it only maintains a discharge capacity of 39.2 mAh/g (Fig. S3b in Supporting information). The corresponding d*Q*/d*V* plots exhibit much worse cycling reversibility during the test. The lower discharge capacity is ascribed to the more intense irreversible electrochemical reaction of the NCM622 active material at higher voltages (Fig. S3c in Supporting information). The Nyquist plots in Fig. S3d (Supporting information) show a similar impedance change after cycling compared with the battery cycled in 3.0–4.3 V (*vs.* Li^+/Li^0). The cycling voltammetry results in Figs. S4a and b (Supporting information) also exhibit increasing potential differences between the reduction and the oxidation peaks, from 0.40 V for the initial cycle to 0.65 V for the 5th cycle, suggesting a poor cyclability.

Typical Li-ion batteries suffer fast performance deterioration at elevated temperatures due to the side reactions and instabilities of the organic liquid electrolytes applied in the batteries [35]. Hence, solid-state battery with solid electrolyte provides the possibility to exhibit excellent electrochemical performances at high operating temperatures. Herein, the fabricated battery using target electrolyte milled after 16 h in this work was also cycled at 0.2 C with different upper cut-off voltages (4.3 and 4.5 V) under 60 °C to investigate the electrochemical performance. As shown in Fig. 4a, those batteries show two charge voltage plateaus at 3.8 V and 4.25 V (*vs.* Li^+/Li^0) during the initial charge process and a discharge voltage of 3.8 V during the subsequent discharge process. In contrast, this battery shows only one charge voltage plateau when the upper cut-off voltage was set at 4.3 V at room temperature, indi-

cating that the appearance of this plateau is associated with the operating temperature. The extra voltage plateau is associated with the hexagonal phase to the new hexagonal phase (H2-H3) for the layered structure cathode materials, which have an obviously improvement during the first cycle under high temperature and are well reported in previous reports [36]. This battery delivers initial discharge capacities of 161.8 mAh/g and 200.8 mAh/g with corresponding coulombic efficiencies of 86.3% and 82.4% when the upper cut-off voltages were set at 4.3 and 4.5 V (*vs.* Li^+/Li^0), respectively, as depicted in Fig. 4b. Those values are much higher than that at room temperature. When the battery was charged to 4.3 V, it shows good cycling performance, and maintains a discharge capacity of 103.1 mAh/g after 90 cycles with capacity retention of 65.6%. In comparison, when the battery was cycled in a wider voltage window with higher cut-off voltage (4.5 V), it shows much worse cyclability and fast capacity degradation. It shows higher discharge capacities than that cycled at 4.3 V in the first 40 cycles and sustains a discharge capacity of 69.5 mAh/g after 90 cycles with a low-capacity retention of 34.6%. To investigate the resistance changes during cycling, EIS before and after 90 cycles of those solid-state batteries cycled at different voltage windows were also performed in Figs. 4c and d. The EIS spectra of battery cycled at 4.5 V exhibits larger interfacial resistance than that cycled at 4.3 V after 90 cycles, suggesting that more side reactions and phase transition occurs at higher upper cut-off voltage. This is also associated with the more obvious charge voltage plateau when cycled at 4.5 V under 60 °C. To evaluate the phase transition of the assembled battery cycled at different operating temperatures, the *dQ/dV* plots of those batteries at chosen cycles are presented in Figs. 4e and f. Comparing with the above section that those batteries cycled at room temperature, the battery here shows an extra d*Q*/d*V* peak during the initial cycle. Those two *dQ/dV* peaks are attributed to the transformation of the M phase to the H1 phase and the hexagonal phase to another hexagonal phase (H2-H3) for the layered NCM622 cathode, which agrees well with the previous charging platforms. As shown in Figs. S4c and d (Supporting information), the CV curves display more obvious redox peaks at higher operating temperatures (60 °C), indicating that the transition is partly affected by the operating temperatures. This is associated with the intrinsic instability of the active materials at elevated temperatures. In Generally, the transition from the H2 phase to the H3 phase is considered to an irreversible phase transition process, which is associated with the fast capacity degradation and the low initial coulombic efficiency at the higher upper cut-off voltage.

In summary, a large-scale $Li_{2.25}Zr_{0.75}Fe_{0.25}Cl_6$ electrolyte can be synthesized through a simple mechanical route in a short milling duration (4 h) with comparable ionic conductivity of 0.74 mS/cm at room temperature than long durations (16 h). A subsequent sintering process significantly lowers its Li-ion conductivity. This annealed phase is multiphase which shows obvious impedance changes during the measuring process. Solid-state batteries using different kinds of $Li_{2.25}Zr_{0.75}Fe_{0.25}Cl_6$ electrolytes and $Li_{5.5}PS_{4.5}Cl_{1.5}$ buffer layer combined with $LiNi_{0.6}Mn_{0.2}Co_{0.2}O_2$ cathode and Li-In anode has been constructed. The long duration (16 h) milled $Li_{2.25}Zr_{0.75}Fe_{0.25}Cl_6$ electrolyte shows higher discharge capacities and superior cyclability at room temperature when cycled between 3.0 V and 4.3 V than that obtained from short duration (4 h). Moreover, the former battery delivers higher discharge capacities and good cyclability at the same measuring conditions under 60 °C during 90 cycles. When the upper cut-off voltage rises to 4.5 V, this battery shows superior discharge capacities in the first 40 cycles and fast degradation of capacity in the 90 cycles due to the irreversible phase transition from the H2 phase to the H3 phase for $LiNi_{0.6}Mn_{0.2}Co_{0.2}O_2$ cathode. Our research reveals the milling parameters on the conductivity and electrochemical performances of $Li_{2.25}Zr_{0.75}Fe_{0.25}Cl_6$ electrolyte, which can promote its large-scale of synthesis and applications in all-solid-state batteries.

Declaration of competing interest

The authors declare that they have no conflict of interest.

Acknowledgments

This work was supported by the National Key Research and Development Program (Nos. 2021YFB2500200, 2021YFB2400300) and the National Natural Science Foundation of China (No. 52177214), the Certificate of China Post-doctoral Science Foundation (No. 2019M652634). We gratefully acknowledge the Analytical and Testing Center of HUST for us to use the facilities.

Supplementary materials

Supplementary material associated with this article can be found, in the online version, at doi:10.1016/j.cclet.2022.05.058.

References

[1] J. Janek, W.G. Zeier, Nat. Energy 1 (2016) 16141.
[2] J.C. Bachman, S. Muy, A. Grimaud, et al., Chem. Rev. 116 (2016) 140–162.
[3] G.Y. Adachi, N. Imanaka, S. Tamura, Chem. Rev. 102 (2002) 2405–2430.
[4] K. Park, B.C. Yu, J.W. Jung, et al., Chem. Mater. 28 (2016) 8051–8059.
[5] V.K. Thakur, G. Ding, J. Ma, P.S. Lee, X. Lu, Adv. Mater. 24 (2012) 4071–4096.
[6] J. Ding, R. Xu, C. Yan, et al., Chin. Chem. Lett. 31 (2020) 2339–2342.
[7] N. Kamaya, K. Homma, Y. Yamakawa, et al., Nat. Mater. 10 (2011) 682–686.
[8] L. Peng, C. Yu, Z. Zhang, et al., Chem. Eng. J. 430 (2022) 132896.
[9] Z. Zhang, J. Zhang, H. Jia, et al., J. Power Sources 450 (2020) 227601.
[10] Y. Zhu, X. He, Y. Mo, ACS Appl. Mater. Interfaces 7 (2015) 23685–23693.
[11] Y. Zhu, X. He, Y. Mo, J. Mater. Chem. A 4 (2016) 3253–3266.
[12] L. Peng, H. Ren, J. Zhang, et al., Energy Storage Mater. 43 (2021) 53–61.
[13] Y. Dai, Q. Chen, C. Hu, et al., Chin. Chem. Lett. 33 (2022) 1435–1438.
[14] Z. Zhang, J. Zhang, Y. Sun, et al., J. Energy Chem. 41 (2020) 171–176.
[15] T. Asano, A. Sakai, S. Ouchi, et al., Adv. Mater. 30 (2018) e1803075.
[16] X. Li, J. Liang, J. Luo, et al., Energy Environ. Sci. 12 (2019) 2665–2671.
[17] R. Schlem, S. Muy, N. Prinz, et al., Adv. Mater. 10 (2020) 1903719.
[18] J. Liang, X. Li, S. Wang, et al., J. Am. Chem. Soc. 142 (2020) 7012–7022.
[19] L. Zhou, T.T. Zuo, C.Y. Kwok, et al., Nat. Energy 7 (2022) 83–93.
[20] K. Wang, Q. Ren, Z. Gu, et al., Nat. Commun. 12 (2021) 4410.
[21] H. Kwak, D. Han, J. Lyoo, et al., Adv. Energy Mater. 11 (2021) 2003190.
[22] K.H. Park, K. Kaup, A. Assoud, et al., ACS Energy Lett. 5 (2020) 533–539.
[23] J. Park, D. Han, H. Kwak, et al., Chem. Eng. J. 425 (2021) 130630.
[24] S. Chen, C. Yu, S. Chen, et al., Chin. Chem. Lett. 33 (2022) 4635–4639.
[25] X. Li, J. Liang, N. Chen, et al., Angew. Chem. Int. Ed. 58 (2019) 16427–16432.
[26] C. Wang, J. Liang, J. Luo, et al., Sci. Adv. 7 (2021) eabh1896.
[27] M. Jansen, U. Henseler, J. Solid State Chem. 99 (1992) 110–119.
[28] L. Peng, S. Chen, C. Yu, et al., J. Power Sources 520 (2022) 230890.
[29] S. Zhang, F. Zhao, S. Wang, et al., Adv. Energy Mater. 11 (2021) 2100836.
[30] T. Yu, J. Liang, L. Luo, et al., Adv. Energy Mater. 11 (2021) 2101915.
[31] K. Kim, D. Park, H.G. Jung, et al., Chem. Mater. 33 (2021) 3669–3677.
[32] G. Xu, L. Luo, J. Liang, et al., Nano Energy 92 (2022) 106674.
[33] L.M. Riegger, R. Schlem, J. Sann, et al., Angew. Chem. Int. Ed. 60 (2021) 6718–6723.
[34] L. Peng, C. Yu, Z. Zhang, et al., Energy Environ. Mater. 6 (2023) e12308.
[35] S. Ma, M. Jiang, P. Tao, et al., Prog. Nat. Sci. Mater. Int. 28 (2018) 653–666.
[36] P. Ping, X. Xia, Q.S. Wang, J.H. Sun, J.R. Dahn, J. Electrochem. Soc. 160 (2013) A426–A429.